ChemComm

COMMUNICATION

View Article Online
View Journal | View Issue

Cite this: *Chem. Commun.*, 2015, 51, 16996

Received 1st August 2015,
Accepted 29th September 2015

DOI: 10.1039/c5cc06453h

www.rsc.org/chemcomm

Pre-concentration and energy transfer enable the efficient luminescence sensing of transition metal ions by metal–organic frameworks†

Xinping Lin,‡[a] Yahui Hong,‡[a] Chao Zhang,[a] Ruiyun Huang,[a] Cheng Wang*[a] and Wenbin Lin*[ab]

The 2,2′-bipyridyl moieties lining the channels of two designer metal–organic frameworks (MOFs), UiO-bpydc and Eu-bpydc (bpydc is 2,2′-bipyridine 5,5′-dicarboxylic acid), recognize and pre-concentrate metal ion analytes and, in the case of Eu-bpydc, transfer energy to the Eu^{3+} centers, to provide highly sensitive luminescence sensors for transition metal ions.

The increasing concern about heavy metal pollution in developing countries calls for low-cost, deployable technologies that can detect trace amounts of metal ions. Luminescence-based methods have the potential to meet this need, but their sensitivity must be further improved before they can be adopted for practical applications. Pre-concentration, a process of dynamic enrichment of analytes,[1,2] can be integrated into luminescence-based methods to significantly enhance detection sensitivity.[3]

Metal–organic frameworks (MOFs) are a unique category of porous materials that can be designed and constructed at the molecular level.[4–6] Functional MOFs have been reported to serve as effective luminescence sensors[7–9] for small molecules,[10–16] metal ions,[17,18] anions,[19] protons[20,21] and DNA.[22] In particular, pre-concentration effects have been observed in a few examples,[3,23] in which analytes are selectively absorbed by a porous solid through favorable analyte–MOF interactions, to increase the sensitivities. This pre-concentration effect can be fine-tuned through chemical modifications of the MOF channels.

In this work, we report the use of 2,2′-bipyridyl groups (bpy) in MOFs to optimize the interactions between MOFs and metal ion analytes, leading to much enhanced sensitivities. Moreover, single crystal X-ray structure determination revealed that different coordination modes of the metal ions are responsible for the different ion selectivities of the two MOFs. Confocal microscopy imaging demonstrated the accessibility of the bpy sites in the MOF interior to metal ion analytes.

2,2′-Bipyridine is an effective metal chelator, and tends to coordinate with metal ions during MOF synthesis.[17,24–26] Consequently, few MOFs possess free 2,2′-bipyridine sites inside their porous structures: the UiO MOF constructed from Zr^{4+} and 2,2′-bipyridine 5,5′-dicarboxylic (bpydc) bridging ligands,[27] the MOF-253[28] constructed from Al^{3+} ions and bpydc ligands, and a series of lanthanide MOFs[29] with bpydc as the ligand. In all these examples, the metal ions in the MOF construction were hard acids or had large ionic radii, and cannot chelate with bpy groups under acidic MOF growth conditions. The free bpy sites can be utilized to pre-concentrate other metal ions for efficient luminescence sensing.

We chose UiO-bpydc[27] and Eu-bpydc[29,30] in the present luminescence sensing study. UiO-bpydc is constructed from $Zr_6(\mu_3\text{-}O)_4(\mu_3\text{-}OH)_4(\text{carboxylate})_{12}$ secondary building units (SBUs) and linear bpydc dicarboxylate bridging ligands to afford a porous structure with 3-D open channels. The bpydc ligand serves both as the chelator for ion pre-concentration and as the fluorescence reporter for signal read-out. The superior stability of the UiO structure enabled us to perform metal ion sensing in aggressive solvent systems. The Eu-bpydc is constructed from Eu^{3+} ions and bpydc ligands to form 1-D open channels. Eu^{3+} is a bright red emitter with a narrow emission line width, thus is an ideal luminescence reporter. In the Eu-bpydc MOF, we observed efficient energy transfer from the bpydc to the Eu^{3+}. The metal chelation under the sensing conditions interrupts this energy transfer, leading to sensitive read-out (Fig. 1). The morphology and phase purity of the samples were carefully characterized by Electron Microscopy (EM, Fig. 2a and Fig. S1, ESI†), Powder X-ray Diffraction (PXRD, Fig. 2b) and thermogravimetric analysis (TGA, Fig. S2 and S3, ESI†). Crystals of 200 nm in size for UiO-bpydc and a few microns for Eu-bpydc were used in these studies. The stabilities of the MOFs in the presence of metal ion solutions were confirmed by PXRD studies (Fig. S4 and S5, ESI†).

[a] *College of Chemistry and Chemical Engineering, i-Chem, Xiamen University, Xiamen 361005, P. R. China. E-mail: wangchengxmu@xmu.edu.cn, wenbinlin@uchicago.edu*

[b] *Chemistry Department, University of Chicago, 929 E 57th Street, Chicago, IL 60637, USA*

† Electronic supplementary information (ESI) available: Experimental details, EM image, TGA, UV-Vis, PL, and PXRD. CCDC 1416081 and 1416082. For ESI and crystallographic data in CIF or other electronic format see DOI: 10.1039/c5cc06453h

‡ These authors contribute equally.

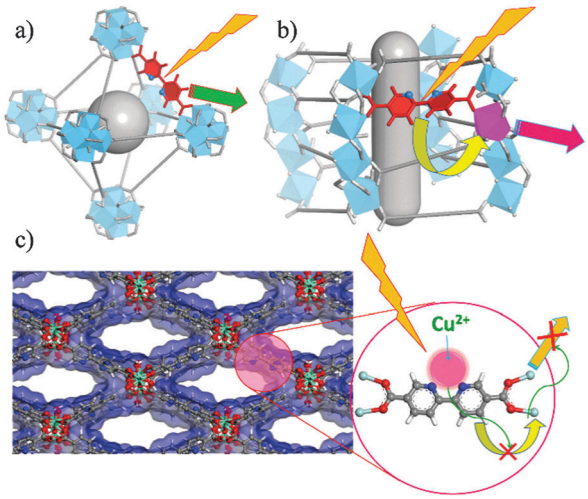

Fig. 1 The crystal structure of the two MOFs with free bpy moieties in the channel. (a) UiO-bpydc; (b) and (c) Eu-bpydc; the scheme in the figures also shows how the metal chelation interrupts energy transfer and emission.

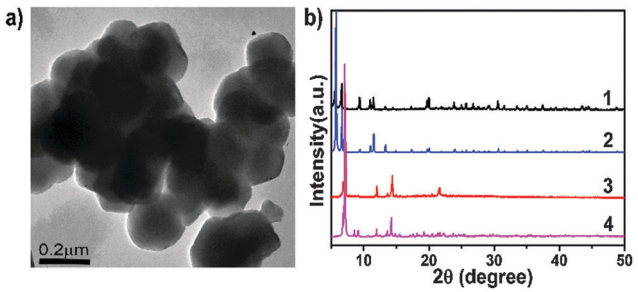

Fig. 2 TEM of UiO67-bpydc (a) and PXRD (b) of the UiO67-bpydc as synthesized (1), simulated from CIF (2) and Eu-bpydc as synthesized (3), simulated from CIF (4).

As expected, Mn^{2+}, Fe^{2+}, Co^{2+}, Ni^{2+}, Cu^{2+}, Zn^{2+}, Cd^{2+}, and Fe^{3+} all quench the luminescence of the two MOFs (Fig. 3b and Fig. S6–S8, ESI†). For UiO-bpydc, Fe^{3+} is the most efficient quencher, while for Eu-bpydc, Cu^{2+} is the most efficient one. The detection limit of Fe^{3+} *via* the luminescence quenching of UiO-bpydc can be as low as 3.2 ppb, while the detection limit for Cu^{2+} by the Eu-bpydc sensor can be lower than 6.4 ppb. These detection limits were 2–3 orders of magnitude lower than those with the corresponding free bpydc ligand as the sensor.

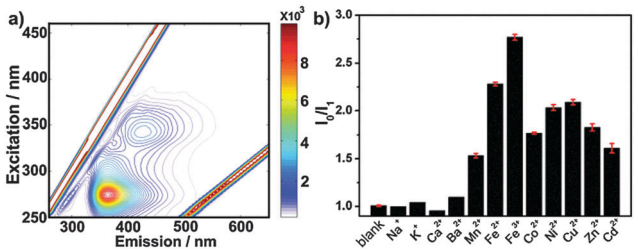

Fig. 3 The 2D fluorescence of the UiO-bpydc (a) and the fluorescence intensity of UiO-bpydc in MeOH solutions in the presence of 4.95 μM of metal ions (b).

Encouraged by the excellent sensitivity of the designer MOF sensors, we proceeded to investigate the underpinnings of the sensing processes. Specifically, we wish to probe the following. (1) Does pre-concentration play a role in the enhanced sensitivity? (2) What is the nature of the MOF luminescence in the quenching study? (3) What is the origin of the different quenching efficiencies of different metal ions? (4) Can the metal ions diffuse into the interior of the MOF crystals, or are they only absorbed at the very surface of the MOF crystal?

To answer the first question, we determined the amounts of metal ions trapped in the MOFs by inductively coupled plasma-optical emission spectroscopy (ICP-OES). After soaking UiO-bpydc in methanol solutions of metal ions (500 μM), the amounts of metal ions inside the MOF channels were determined to correspond to 25–53% of all the bpy sites in the MOF structures, or a pre-concentration factor of 370–1230 times, calculated as the concentration of metal ions in the MOF channel *vs.* the concentration in the solution. Such a local enrichment of the analyte can lead to more sensitive luminescence quenching.

With such an equilibrium between the ions inside the MOF channels and those in the outside solution in mind, we further examined the luminescence quenching of the MOFs at different metal ion concentrations (Fig. S9 and S10, ESI†). The I_0/I_1 values (I_0 and I_1 are the luminescence intensities in the absence and presence of metal ions) were plotted against metal ion concentrations $[M^{n+}]$. For UiO-bpydc, such curves can be fitted to the Stern–Völmer equation $(I_0/I_1) = 1 + K[M^{n+}]$ (Fig. S9 and S10, ESI†), a line intercepting the y-axis at 1 with a slope of K, where K is the Stern–Völmer constant. This constant K represents the quenching sensitivity, and is up to $(3.0 \pm 0.2) \times 10^5\ M^{-1}$ for Fe^{3+}, corresponding to a detection limit of 3.2 ppb under the current signal/noise ratio (Table 1). Similarly the detection limit of Cu^{2+} by Eu-bpydc is found to be below 6.4 ppb (Fig. 4).

We attributed this pre-concentration and luminescence quenching to the chelation capability[31] of the free bpy moieties. Consistent with this, the alkaline earth metals do not have much effect on the MOF luminescence, because of their lower affinity toward bpydc. In addition, if metal chelation is the main source of luminescence quenching, static quenching mechanism is expected, in which analytes pre-associated with the sensor molecules at the ground state. The dynamic quenching mechanism, on the other hand, requires a diffusion of the quencher to find the excited sensor molecule and to quench the luminescence.

Table 1 The Stern–Völmer constants, pre-concentration factors and detection limits for UiO-bpydc with different metal quenchers

Metal ions	K_{sv} $[\times 10^5\ M^{-1}]$	Pre-concentration factor	Detection limit for MOF (ppb)	Detection limit for ligand (ppb)
Mn^{2+}	1.01 ± 0.06	492	9.4	2400
Fe^{2+}	2.4 ± 0.2	517	4.1	2600
Fe^{3+}	3.0 ± 0.2	1095	3.2	600
Co^{2+}	1.50 ± 0.06	374	6.8	2000
Ni^{2+}	1.6 ± 0.1	1207	6.5	600
Cu^{2+}	1.8 ± 0.1	1232	6.0	400
Zn^{2+}	1.53 ± 0.07	535	7.4	350
Cd^{2+}	1.23 ± 0.07	372	15.8	1700

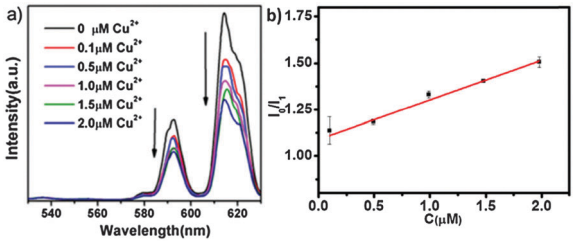

Fig. 4 The fluorescence of the Eu-bpydc (a) and the Stern–Völmer plot of the Eu-bpydc with various concentration of Cu^{2+} under λ = 325 nm (b).

These two mechanisms can be differentiated by a luminescence lifetime study: dynamic quenching will show a comparable decrease in lifetime, while static quenching does not change the lifetime. We measured the fluorescence lifetime of UiO-bpydc with different Fe^{3+} ion concentrations, and did not observe any change in the weighted lifetimes (Fig. S11, ESI†). This result is consistent with static quenching, supporting the model of chelated metal ions as the quenching sites.

To reveal more information about the nature of the excited states that are quenched by the metal ions, the emission spectra of the UiO-bpydc suspensions were recorded by systematically changing the excitation wavelengths. The datasets were compiled into a 2D map with the luminescence intensities encoded by different colors (Fig. 3a and Fig. S12, ESI†). The peaks at $\lambda_{ex} \approx 275$ nm and $\lambda_{em} \approx 365$ nm are attributed to the ligand π–π^* transition, because the peak positions only change slightly in different solvents. In contrast, the peaks at $\lambda_{ex} \approx 340$ nm and $\lambda_{em} \approx 425$ nm significantly shift in different solvents (Fig. 3a and Fig. S12, ESI†) and are thus attributed to the n–π^* transition of the ligand. The emission peak used in the metal ion sensing is the π–π^* peak.

UiO-bpydc emits signals at the UV wavelength, which are not directly readable to the naked eye. To overcome this drawback, the Eu-bpydc MOF can emit bright red light due to efficient energy transfer from bpydc to Eu^{3+}. The strong red emission at 592 and 617 nm, characteristic of the $^5D_0 \rightarrow {}^7F_1$ and $^5D_0 \rightarrow {}^7F_2$ transitions of Eu^{3+}, were used in the sensing study (Fig. 4). The bpydc-to-Eu^{3+}energy transfer can be confirmed by the Eu^{3+} luminescence excitation spectrum shown in Fig. S13 (ESI†), in which the excitation peak at around 300 nm coincides with the broad absorption spectrum of the bpydc ligand (Fig. S13, inset; Fig. S14, ESI†), instead of the sharp excitation lines of Eu^{3+} (Fig. S15, ESI†). It is also worth noting that Eu^{3+} itself absorbs light poorly as compared to that of bpydc, because of the forbidden nature of the f–f transitions. Only such a combination of bpydc as the light-harvesting antenna and Eu^{3+} as the emitter in the visible range gives a bright luminescence assembly for efficient sensing. The chelation of metal ions to bpydc interrupts the bpydc-to-Eu^{3+} energy transfer, and quenches the MOF luminescence.

The quenching of the MOF luminescence by metal ions can be due to multiple reasons: redox reaction, intersystem crossing to triplet states and vibration-assisted non-radiative relaxation. Different metals can thus quench the MOF luminescence to different degrees. Upon comparing the sensitivities of the UiO-bpydc and Eu-bpydc towards the same metal ion, a significant difference can be identified. In particular, Cu^{2+} gives a relatively high quenching response in the Eu-bpydc MOF, but not in UiO-bpydc. We hypothesized that in the Eu-bpydc structure, two adjacent bpy moieties are close enough to coordinate to the same metal ion in a square planar geometry. Such different coordination motifs can lead to different ion selectivity. To test this hypothesis, we tried to perform single-crystal to single-crystal metallation of the Eu-bpydc by soaking the single crystal in Cu^{2+} solution. Unfortunately, the Cu(II) position in this X-ray diffraction dataset cannot be positively identified, due to the low occupancy of Cu(II) (22% bpy sites coordinated with Cu(II) as determined by ICP-OES). Instead, a dataset of the crystal soaked in Cu^{+} solution confidently gives the positions of the coordinated metals.[32] The crystal structure of Cu(I) clearly showed a combination of square planar coordination sites from two adjacent bpy moieties and mono-coordination sites with only one bpy ligand (60% bpy sites coordinated with Cu(I) as determined by ICP-OES) (Fig. 5). This observation reveals the detailed coordination motif as a reason for ion selectivity.

While the metal coordination equilibrium can affect the sensitivity of the sensors, diffusions of the metal ions into the MOFs are important to the response speed of the sensors. The luminescence signals can reach steady states in less than one minute in our sensing experiments after the addition of the analytes in methanol or DMF solutions (Fig. S16, ESI†). In other cases, the diffusion can be much slower. For example, we also performed metal sensing using UiO-bpydc in aqueous suspensions. Instead of quenching, Zn^{2+} and Cd^{2+} significantly enhanced the MOF fluorescence, possibly due to the suppression of deactivation pathways of the n $\rightarrow$ π^* state (Fig. S17, ESI†). This result is of considerable interest for the sensing of Cd^{2+} in an aqueous environment. However, the diffusion of the metal ions in the MOF channels in aqueous solution was very slow due to the large hydration radii of the metal ions, and only reached equilibrium after 12 hours.

To develop faster MOF sensors, we would like to know how far can the metal ions diffuse into the MOF crystal and how fast can this happen. To do this, we monitored the luminescence image of a single crystal of Eu-bpydc by confocal microscopy after the addition of the Cu^{2+} quencher in DMF (Fig. 6). As Cu^{2+} diffuses into the crystal, the luminescence of the MOF decreases continuously. The degrees of luminescence quenching on different parts of the

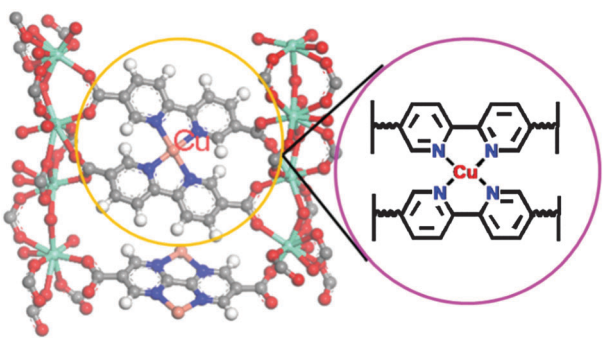

Fig. 5 The crystal structure of Eu-bpydc-Cu(I) crystal.

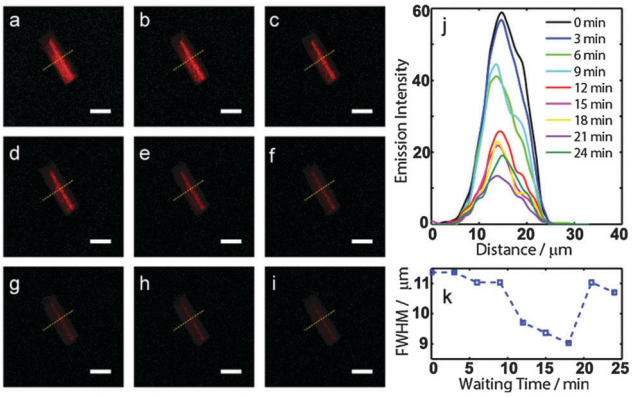

Fig. 6 Confocal fluorescence microscopy images of the Eu-bpydc crystal with Cu^{2+} DMF solutions as the quencher. (The images from (a) to (i) were taken every three minutes; the scale bar is 20 μm); (j) emission intensity profiles along the yellow line on the images across the crystal; (k) full width at half maximum of the emission intensity profiles in (j) at different times of quencher diffusion.

images are related to the distributions of local Cu^{2+} concentrations. We have plotted the luminescence intensity profile across the crystal in Fig. 6j at different times. As Cu^{2+} diffuses from the outside to the interior of the crystal, the intensity profile should first become narrower and narrower, because the outside part of the crystal is quenched by the Cu^{2+} but the interior has not been reached yet. However, if the Cu^{2+} can finally diffuse into the very interior of the crystal and reach equilibrium, the width of the luminescence intensity profile will become wider again in the final step, as all parts of the crystal are in equilibrium and equally quenched, and the remaining luminescence should represent the size of the crystal again. To better visualize the width of the emission intensity profile in Fig. 6j, we have plotted the full width at half maximum (FWHM) of the intensity profiles at different diffusion times in Fig. 6k. The FWHM exhibited the expected decreasing and recovery behaviour as a function of time, verifying that the metal ion can diffuse into the center of the MOF crystal under the experimental conditions. This observed diffusion into the MOF single crystal is much slower than that of the micro-crystal used in the luminescence sensing due to the different sizes of the crystals.

We have designed two MOFs with free 2,2′-bipyridine moieties as chelating sites lining the MOF channels for efficient metal ion sensing. The pre-concentration of the metal ions inside these MOF channels gives a significant enhancement of the analytical sensitivity. In the Eu-bpydc MOF, a bpydc-to-Eu energy transfer also gives the bright visible emission for sensitive detection. Such a compact design of light-absorbing antenna, energy transfer, chemical recognition and pre-concentration highlights MOFs as an excellent platform to produce highly efficient and specific sensing materials.

This work was supported by the National Natural Science Foundation of P. R. China (21471126), the National Thousand Talents Program of P. R. China, the 985 Program of the Chemistry and Chemical Engineering disciplines of Xiamen University.

Notes and references

1 K. E. Shafer-Peltier, C. L. Haynes, M. R. Glucksberg and R. P. Van Duyne, *J. Am. Chem. Soc.*, 2003, **125**, 588–593.
2 T. M. Swager, J. Im, A. R. Petty, J. Schnorr and C. Schmaedicke, *PCT Int. Appl.*, 2015, WO 2015035243 A1 20150312.
3 M. Carboni, Z. Lin, C. W. Abney, T. Zhang and W. Lin, *Chem. – Eur. J.*, 2014, **20**, 14965–14970.
4 C. Wang, D. Liu and W. Lin, *J. Am. Chem. Soc.*, 2013, **135**, 13222–13234.
5 D. Liu, K. Lu, C. Poon and W. Lin, *Inorg. Chem.*, 2014, **53**, 1916–1924.
6 K. K. Tanabe and S. M. Cohen, *Chem. Soc. Rev.*, 2011, **40**, 498–519.
7 L. E. Kreno, K. Leong, O. K. Farha, M. Allendorf, R. P. Van Duyne and J. T. Hupp, *Chem. Rev.*, 2012, **112**, 1105–1125.
8 Z. Hu, B. J. Deibert and J. Li, *Chem. Soc. Rev.*, 2014, **43**, 5815–5840.
9 M. D. Allendorf, C. A. Bauer, R. K. Bhakta and R. J. T. Houk, *Chem. Soc. Rev.*, 2009, **38**, 1330–1352.
10 J.-M. Zhou, W. Shi, H.-M. Li, H. Li and P. Cheng, *J. Phys. Chem. C*, 2014, **118**, 416–426.
11 A. Lan, K. Li, H. Wu, D. H. Olson, T. J. Emge, W. Ki, M. Hong and J. Li, *Angew. Chem., Int. Ed.*, 2009, **48**, 2334–2338.
12 R.-B. Lin, F. Li, S.-Y. Liu, X.-L. Qi, J.-P. Zhang and X.-M. Chen, *Angew. Chem., Int. Ed.*, 2013, **52**, 13429–13433.
13 M.-J. Dong, M. Zhao, S. Ou, C. Zou and C.-D. Wu, *Angew. Chem., Int. Ed.*, 2014, **53**, 1575–1579.
14 N. Yanai, K. Kitayama, Y. Hijikata, H. Sato, R. Matsuda, Y. Kubota, M. Takata, M. Mizuno, T. Uemura and S. Kitagawa, *Nat. Mater.*, 2011, **10**, 787–793.
15 M. G. Campbell, D. Sheberla, S. F. Liu, T. M. Swager and M. Dincă, *Angew. Chem., Int. Ed.*, 2015, **54**, 4349–4352.
16 J.-M. Zhou, W. Shi, N. Xu and P. Cheng, *Inorg. Chem.*, 2013, **52**, 8082–8090.
17 B. Chen, L. Wang, Y. Xiao, F. R. Fronczek, M. Xue, Y. Cui and G. Qian, *Angew. Chem., Int. Ed.*, 2009, **48**, 500–503.
18 K.-K. Yee, N. Reimer, J. Liu, S.-Y. Cheng, S.-M. Yiu, J. Weber, N. Stock and Z. Xu, *J. Am. Chem. Soc.*, 2013, **135**, 7795–7798.
19 B. Chen, L. Wang, F. Zapata, G. Qian and E. B. Lobkovsky, *J. Am. Chem. Soc.*, 2008, **130**, 6718–6719.
20 C. He, K. Lu and W. Lin, *J. Am. Chem. Soc.*, 2014, **136**, 12253–12256.
21 H.-L. Jiang, D. Feng, K. Wang, Z.-Y. Gu, Z. Wei, Y.-P. Chen and H.-C. Zhou, *J. Am. Chem. Soc.*, 2013, **135**, 13934–13938.
22 H.-T. Zhang, J.-W. Zhang, G. Huang, Z.-Y. Du and H.-L. Jiang, *Chem. Commun.*, 2014, **50**, 12069–12072.
23 M. M. Wanderley, C. Wang, C.-D. Wu and W. Lin, *J. Am. Chem. Soc.*, 2012, **134**, 9050–9053.
24 Y.-W. Li, J.-R. Li, L.-F. Wang, B.-Y. Zhou, Q. Chen and X.-H. Bu, *J. Mater. Chem. A*, 2013, **1**, 495–499.
25 Q. Tang, S. Liu, Y. Liu, J. Miao, S. Li, L. Zhang, Z. Shi and Z. Zheng, *Inorg. Chem.*, 2013, **52**, 2799–2801.
26 M. Zheng, H. Tan, Z. Xie, L. Zhang, X. Jing and Z. Sun, *ACS Appl. Mater. Interfaces*, 2013, **5**, 1078–1083.
27 L. Li, S. Tang, C. Wang, X. Lv, M. Jiang, H. Wu and X. Zhao, *Chem. Commun.*, 2014, **50**, 2304–2307.
28 E. D. Bloch, D. Britt, C. Lee, C. J. Doonan, F. J. Uribe-Romo, H. Furukawa, J. R. Long and O. M. Yaghi, *J. Am. Chem. Soc.*, 2010, **132**, 14382–14384.
29 M. Gustafsson, J. Su, H. Yue, Q. Yao and X. Zou, *Cryst. Growth Des.*, 2012, **12**, 3243–3249.
30 H. Liu, X. Peng and H. Zeng, *Inorg. Chem. Commun.*, 2014, **46**, 39–42.
31 M. K. Milčić, V. B. Medaković, D. N. Sredojević, N. O. Juranić and S. D. Zarić, *Inorg. Chem.*, 2006, **45**, 4755–4763.
32 Crystal structures of Eu-bpydc ($P2_1/c$ a = 26.238(2) b = 14.188(2) c = 16.859(1) β = 98.014° CCDC 1416081) and Eu-bpydc-Cu(I) ($P2_1/c$ a = 26.531(2) b = 13.617(4) c = 16.407(2) β = 98.04° CCDC 1416082).